



Research articles

Magnetic structure of magnetoelectric multiferroic HoFeWO₆C. Dhital^{a,*}, R.L. Dally^b, D. Pham^a, T. Keen^a, Q. Zhang^c, P. Siwakoti^d, R. Nepal^d, R. Jin^{d,e}, R. Rai^f^a Department of Physics, Kennesaw State University, Marietta, GA 30060, USA^b NIST Center for Neutron Research, National Institute of Standards and Technology, Gaithersburg, MD 20899-6102, USA^c Neutron Scattering Division, Oak Ridge National Laboratory, Oak Ridge, TN 37831, USA^d Department of Physics and Astronomy, Louisiana State University, Baton Rouge, LA 70803, USA^e Department of Physics and Astronomy, University of South Carolina, Columbia, SC 29208, USA^f Department of Physics, SUNY Buffalo State, Buffalo, NY 14222, USA

ARTICLE INFO

Keywords:

Magnetism
Magnetic structure
Neutron diffraction
Magnetoelectric coupling

ABSTRACT

The polar magnetic oxide, HoFeWO₆, is synthesized, and its crystal structure, magnetic structure, and thermodynamic properties are investigated. HoFeWO₆ forms the polar crystal structure (space group *Pna*2₁ (#33)) due to the cation ordering of W⁶⁺ and Fe³⁺. An antiferromagnetic transition at $T_N = 17$ K is accompanied by a significant change in magnetic entropy with a value of ≈ 5 J kg⁻¹ K⁻¹ in a 70 kOe applied field. Temperature dependent neutron diffraction and magnetization data indicate that the Fe sublattice orders in a strongly non-collinear and non-coplanar arrangement below T_N . The Fe ordering initially leads to induced ordering of the Ho spins such that the Ho spins also show behavior of long-range ordering that is evident from the neutron diffraction measurements. Below $T \approx 4$ K, the Ho spins order independently and pull the Fe spins toward the direction of Ho spins. A comparison with the magnetic structures and corresponding ferroelectric properties of other members of RMWO₆ ($R = Y, Sm-Tm, M = Cr, Fe, V$) family indicate that the spontaneous polarization is due to the magnetic structure specific to the Fe sublattice through magnetoelectric coupling whereas the polarization is independent of the Ho sublattice.

1. Introduction

Magnetoelectric multiferroic materials are magnetic insulators having simultaneous and coupled ferroelectric polarization and magnetization [1–6]. Depending upon the origin of the ferroelectric polarization, these materials are generally classified as type I or type II multiferroics [1–6]. In type I multiferroics, such as BiFeO₃ [7] and YMnO₃ [8], the ferroelectric order arises from the polar distortion of non-magnetic ions at high temperature whereas the magnetism sets in at low temperature due to the magnetic ions. The separate origin and transition temperatures for ferroelectricity and magnetism lead to weak coupling between the two order parameters [9–14]. Type-II multiferroics have a non-polar crystal structure in the paramagnetic phase, and magnetic ordering with specific spiral or non-collinear spin structures breaks the inversion symmetry and thus, induces ferroelectricity that couples strongly with the magnetism [10–13]. The requirement of complicated magnetic structures makes type-II multiferroics rare and requires low temperatures for the magnetic interactions to become

appreciable to generate such structures [13]. In general, whether it be type I or type II, the seemingly antagonistic requirements for ferroelectric and magnetic order makes magnetoelectric multiferroic materials rare in nature [11–12]. Therefore, there has been a continuous effort to find new candidate materials to increase the magnetoelectric coupling and the working temperature.

One way to form a polar crystal structure is via chemical ordering. Therefore, chemically ordered polar magnetic insulators are perfect candidates for magnetoelectric multiferroic materials, such as M₂Mo₃O₈ ($M = Fe, Mn$) [15–17], CaBaCo₄O₇ [18–20], Ni₃TeO₆ [21–22] and RFeWO₆ ($R = Y, Sm-Tm$) [23–26]. These compounds stabilize in a polar structure right at the formation temperature due to chemical or charge ordering and do not undergo a structural transition from a non-polar paraelectric to a polar phase as in type I materials. Such polar materials remain pyroelectric at all temperatures. In these materials, a magnetic field dependent change in polarization (ΔP) occurs at the magnetic ordering temperature indicating magnetoelectric multiferroic behavior. These materials are also classified as type-III multiferroics

* Corresponding author.

E-mail address: cdhital@kennesaw.edu (C. Dhital).<https://doi.org/10.1016/j.jmmm.2021.168725>

Received 25 August 2021; Received in revised form 4 October 2021; Accepted 23 October 2021

Available online 30 October 2021

0304-8853/© 2021 Elsevier B.V. All rights reserved.

because they do not undergo any structural transition and do not require complicated magnetic structures [24]. These chemically ordered polar systems are promising candidates for high temperature multiferroic materials because complex magnetic ordering is often a result of magnetic frustration at low temperature. Furthermore, being pyroelectric at all temperatures, these materials may only require a small polling field to study the ferroelectric behaviors [23–26].

In the above list of chemically ordered polar oxides, the RMWO₆ [M = Cr, Fe, V] family is rather new. The polar structure is formed right at the formation temperature (1000–1200 °C) with no structural transitions observed below. This means all these compounds are polar even at room temperature [23–31]. At room temperature, all these materials are pyroelectric with immeasurably small switchable polarizations. Below the magnetic ordering temperature, only M = Fe compounds exhibit measurable magnetic field dependent electric polarization [23–26]. This indicates there is significant magnetoelectric coupling in the Fe compounds. In addition to the observation of polarization, the magnetic behavior of these compounds, including the magnetocaloric properties, exhibits interesting properties due to interplay of *3d-4f* magnetism and the single ion anisotropy of the rare earth ions [27–31]. These facts indicate the importance of studying the detailed crystal and magnetic structure evolution of these compounds around and below the magnetic transition to make connections to their observed multiferroic properties. This work presents the detailed temperature evolution of the magnetic structure and associated magnetic behavior of one such compound, HoFeWO₆, by using magnetization, specific heat, dielectric, and neutron powder diffraction measurements. Our observations indicate that Fe³⁺ (*3d⁵*) moments are ordered below the antiferromagnetic transition temperature $T_N \sim 17$ K and these ordered Fe moments induce moments on Ho³⁺ (*4f¹⁰*) moments at the same temperature. Although ordering of Fe and induced ordering of Ho occurs at 17 K, a full moment is developed on Fe around 12 K and Ho at 2 K. Between 17 K and 2 K there is interplay between Fe and Ho moments causing a broad peak in the susceptibility and relatively large magnetic entropy change. The Fe moments order in strong non-collinear and non-coplanar arrangement at T_N and immediately induce moments on Ho. As the temperature is decreased, the Ho moments monotonically increase in value and achieve the maximum value of 8.7 μ_B at 2 K. At 2 K, both Ho and Fe moments mostly lie in the *bc* plane due to interaction between Fe and Ho. The data imply that the observed magnetoelectric properties of this compound are primarily governed by the magnetic structure of the Fe site and the interaction between the Ho and Fe sites.

2. Experiment

Polycrystalline samples of HoFeWO₆ were prepared by using a conventional two-step solid-state reaction. In the first step, Ho₂O₃ and Fe₂O₃ (Alfa Aesar, purity > 99%) were mixed using a mortar and pestle and reacted at 1300 °C with intermediate grinding until a pure phase of HoFeO₃ was obtained. After this, stoichiometric amounts of HoFeO₃ and WO₃ were reacted between 1000 °C and 1020 °C for 24 h in a sealed quartz tube under vacuum. The initial phase screening was performed using a Miniflex Rigaku X-ray diffractometer where HoFeWO₆ was observed as the major phase with a minor (less than 2%) unidentified impurity phase. The temperature dependent neutron powder diffraction data were collected using bank-2 (central wavelength 1.5 Å) and bank-3 (central wavelength 2.665 Å) of the Time of Flight (TOF) powder diffractometer (POWGEN) at the Spallation Neutron Source (SNS), Oak Ridge National Laboratory (ORNL). Due to the involvement of neutron absorbing element Ho in HoFeWO₆, we conducted the neutron absorption corrections on the neutron data pixel by pixel. The Rietveld analysis on the absorption corrected data was performed using FullProf [32]. The magnetic properties were measured using a vibrating sample magnetometer (VSM) and magnetic properties measurement system (MPMS) from Quantum Design. Specific heat was measured using Quantum Design Physical Property Measurement System (PPMS). For the

capacitance measurement, the powder was pressed using a pellet press and annealed at 900 °C for 6 h. A small rectangular piece (≈ 3 mm \times 2 mm \times 0.5 mm) was cut from the pellet and a layer of silver epoxy was placed on two opposite flat surfaces. Gold wire electrodes were attached and the capacitance was measured using an Agilent E4980 AL LCR meter. The sample was placed inside a closed cycle Janis cryostat and the temperature was varied. Where indicated, error bars, uncertainties, and confidence intervals represent plus and minus one standard deviation.

3. Results and discussion

3.1. Crystal structure determination

Fig. 1 shows the observed intensity (I_o), calculated Rietveld refined intensity (I_c), difference ($I_o - I_c$), and nuclear Bragg peak positions for the neutron powder diffraction data at 300 K. The profile parameters were fixed to the instrument resolution while the isotropic thermal factors, atomic coordinates, and lattice parameters were refined. The crystal structure was determined to be the polar orthorhombic space group $Pna2_1$ (#33) with the lattice parameters $a = 10.9703(2)$ Å, $b = 5.1684(3)$ Å, $c = 7.3324(5)$ Å, $V = 415.73(5)$ Å³ and $Z = 4$. The inset of Fig. 1 shows that HoFeWO₆ has a three-dimensional crystal structure consisting of edge sharing pairs of WO₆ and FeO₆ octahedra, similar to HoCrWO₆ [28]. This result is consistent with the previously reported polar crystal structure of DyFeWO₆ [23], which is to be expected due to the similar ionic radii of Dy³⁺ and Ho³⁺. The structure of HoFeWO₆ can be taken to be derived from the euxenite (*Pbcn*) type Ho(TaTi)O₆ or aeschynite (*Prma*) type Dy(TaTi)O₆ [33] compounds. In the euxenite or aeschynite type oxides, the disordered Ta or Ti ions randomly occupy the unique *8d* crystallographic site [33]. In the case of HoFeWO₆, the *8d* crystallographic site splits into two *4a* octahedral sites, where W⁶⁺ and Fe³⁺ are ordered. The origin of such cation ordering lies in the difference in the octahedral distortion parameter $\Delta = \frac{1}{6} \sum_i \left(\frac{d_i - d_m}{d_m} \right)^2$ between the FeO₆ and WO₆ octahedra. Here, d_i is the individual bond length and d_m is the average bond length between the Fe³⁺ or W⁶⁺ cation and the oxygen anions ($\Delta = 0.0026$ for WO₆ and $\Delta = 0.0013$ for FeO₆). The W-O bond distances vary from 1.81 Å to 2.13 Å, the Fe-O bond distances vary from 1.95 Å to 2.13 Å, and the Ho-O distances vary from 2.28 Å to 2.45 Å. The average valence of Ho, Fe, and W were found to be 3.05, 2.92, and 5.98, respectively, by using bond valence sum (BVS) calculations. The crystal structure of HoFeWO₆ viewed along the *a*- and *c*-axis is presented in supplementary section [34] Fig. S1.

3.2. Magnetic, dielectric, and thermodynamic properties

The magnetic, dielectric, and thermodynamic properties of HoFeWO₆ are presented in Fig. 2. Fig. 2a shows the field cooled (FC) dc magnetic susceptibility (χ) under a field of $H = 1$ kOe as a function of temperature, T . The first anomaly occurs at the magnetic ordering temperature $T_N \approx 17$ K. Upon further cooling, $\chi(T)$ increases and exhibits a broad maximum around $T^* \approx 10$ K and small anomaly at $T^{**} \approx 4$ K near the rare earth ordering regime. A broad feature such as this typically occurs in low dimensional magnetic systems and could be related to the arrangement of Ho³⁺ ions as they form quasi-one-dimensional chains along the *c*-axis [25]. The χ - T curve for HoFeWO₆ is similar to that of HoCrWO₆ [28] and other compounds of this family [23–31] where both the rare earth and transition metal sublattices were found to be ordered below T_N . Fitting the magnetic susceptibility, χ , to the Curie-Weiss law [35], $\frac{1}{\chi} = \left(\frac{1}{C} \right) T - \left(\frac{\theta}{C} \right)$ in the temperature range of 300 K to 35 K results in the Curie-Weiss constant $C = 17(1)$ emu-K/mol-Oe and the Curie-Weiss temperature $\theta = -21(3)$ K. The negative Curie-Weiss temperature indicates antiferromagnetic ordering at T_N . From the

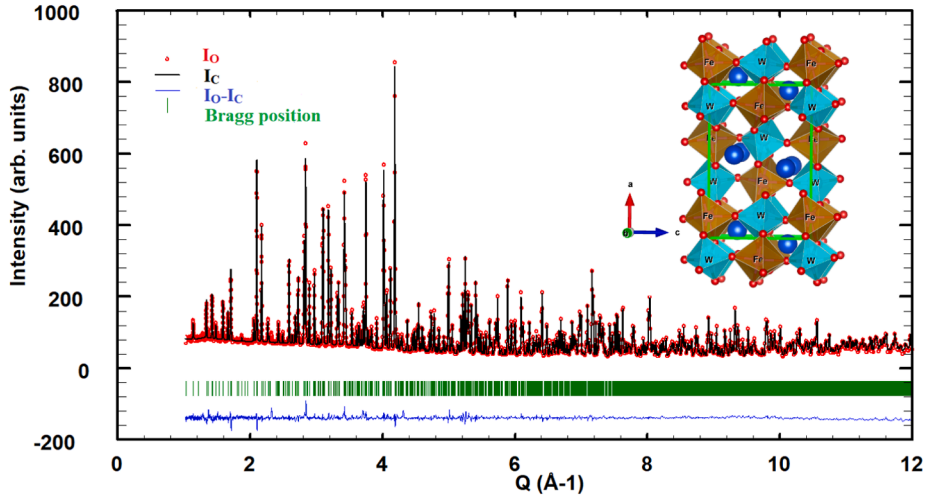


Fig. 1. Room temperature ($T = 300$ K) neutron powder diffraction data. The crystal structure was determined via Rietveld refinement of the observed data (I_0), shown as red dots. The calculated intensity (I_c), difference ($I_0 - I_c$), and nuclear Bragg peak positions are shown as the solid black line, solid blue line, and green tick marks, respectively. The inset shows the crystal structure of HoFeWO_6 viewed along b -axis.

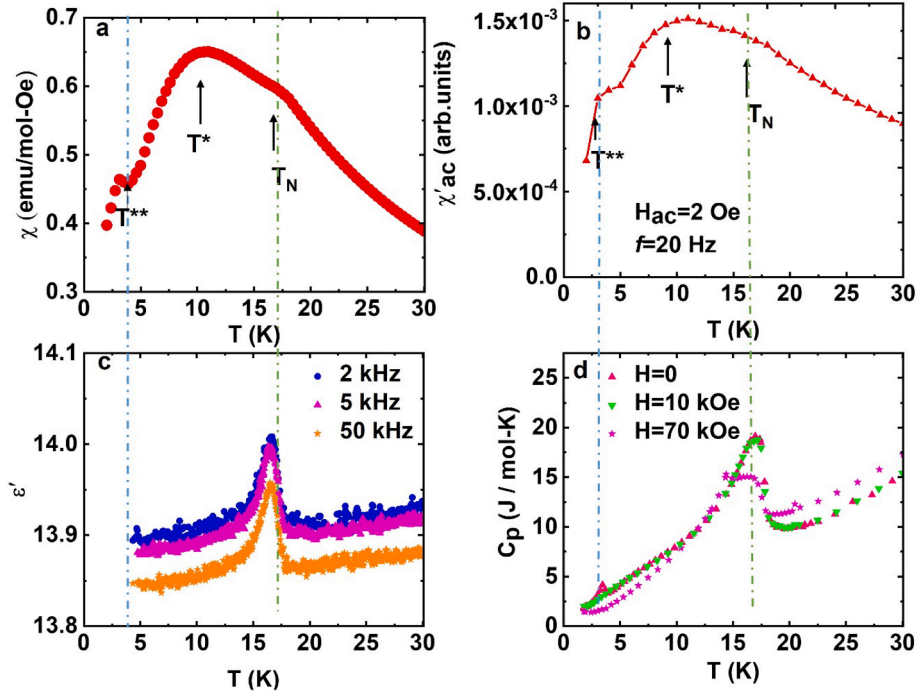


Fig. 2. Magnetic, dielectric, and thermal properties of HoFeWO_6 . (a) Field cooled (FC) magnetic susceptibility, χ , versus temperature, T , measured at $H = 1$ kOe ($1 \text{ Oe} = (1000/4\pi) \text{ A/m}$, $1 \text{ emu}/(\text{mol-Oe}) = 4\pi \times 10^{-6} \text{ m}^3/\text{mol}$). (b) Real part of ac susceptibility, χ'_{ac} , as a function of T . (c) Real part of dielectric constant, ϵ' , as a function of T at different frequencies. (d) Heat capacity, C_p , as function of T at different fields. The dashed lines are a guide to the eye for identification of inflection points.

Curie-Weiss constant, the effective moment is calculated to be $11.62 \mu_B/\text{f.u.}$ (where f.u. is formula unit). This is close to the expected sum of the free ion effective moments of Ho^{3+} ($10.61 \mu_B$) and Fe^{3+} ($5.92 \mu_B$) with

$$\mu_{eff} = \sqrt{\left(\mu_{eff}^{\text{Fe}^{3+}}\right)^2 + \left(\mu_{eff}^{\text{Ho}^{3+}}\right)^2} = 12.15 \mu_B/\text{f.u.}$$

Fig. 2b shows the variation of χ'_{ac} with temperature measured at $f = 20$ Hz. There is a broad peak around the magnetic transitions indicating the significant spin fluctuations and the spin reorientation process. The ac susceptibility decreases at low temperature indicating fully ordered magnetic state with reduced spin fluctuations. We also observed small anomaly in the ac susceptibility, denoted as T^{**} , around 4 K which is the typical rare earth ion ordering regime. This indicates that the Ho ions order on their own and attain their saturated moment value below this

temperature. **Fig. 2c** presents the variation of the real part of the dielectric constant, ϵ' , with temperature measured at three different frequencies: 2 kHz, 5 kHz, and 50 kHz. There is a sharp upturn in ϵ' concurrent with the antiferromagnetic transition T_N and the onset of long-range electric polarization as reported in [25]. Such behavior is often observed in type II multiferroic materials where there is relatively strong magnetolectric coupling [25,36].

The position of the peak does not change with the frequency indicating absence of any relaxation phenomena. **Fig. 2d** presents the Specific heat of HoFeWO_6 as a function of temperature. There is clear λ -type anomaly at the magnetic transition temperature T_N indicating a long-range second order magnetic transition. The λ -type anomaly is suppressed with the application of magnetic field indicating the

destabilization of antiferromagnetic ordering due to applied field. There is also a small λ -type anomaly at $T^{**} \approx 4$ K which is concurrent with the anomaly in the dc susceptibility and the real part of the ac susceptibility. Such an anomaly is generally associated with the rare earth spin dynamics and was also reported in TbFeWO_6 [23]. We will discuss these observations with respect to the temperature dependent neutron diffraction data in the following sections.

The magnetic field dependence of the magnetization $M(H)$ at different temperatures is shown in Fig. 3a. At $T > T_N$, the magnetization exhibits a linear H dependence, consistent with the paramagnetic phase. Non-linear M versus H curves are observed below T_N , suggesting a canted antiferromagnetic phase. At 2 K (red curve), there is a step like behavior in the $M(H)$ curve, indicating a metamagnetic transition. Fig. 3b presents the variation of dM/dH and χ' with magnetic field in the low temperature regime ($T < 4$ K). At $T = 2$ K, there are clearly two distinct anomalies ($H_1 \approx 1.2$ kOe and $H_2 \approx 1.8$ kOe) in both dM/dH and χ' . The fields H_1 and H_2 correspond to the onset and completion of a metamagnetic transition. At 4 K and above, the two anomalies merge and form a single broad peak. Since the two-peak structure in dM/dH only occurs below 4 K, a relationship to the Ho spins can be inferred. Furthermore, the value of the magnetization at 50 kOe and 2 K ($\approx 5\mu_B/f.u.$) is less than that predicted by the Curie-Weiss law. While it shows nearly saturated ferromagnetic type behavior at 2 K in high field, the saturation magnetization is significantly smaller than the expected sum of Fe^{3+} and Ho^{3+} free ion moments. This is unusual in such an insulating system. This indicates the presence of some unsaturated magnetic

moments and/or the averaging of moments in different crystallographic directions due to magnetic anisotropy.

3.3. Magnetocaloric properties

In addition to the magnetoelectric properties, the magnetocaloric properties of this compound are also interesting and worth investigating because of the non-hysteretic second order magnetic phase transition. We have investigated the magnetocaloric properties of HoFeWO_6 by calculating the change in magnetic entropy, ΔS_M . By measuring magnetization versus temperature (70 K-4 K) at different magnetic fields and rearranging the data, we have estimated the change in the magnetic entropy using relation [37],

$$\Delta S(T, 0 \rightarrow H) = \int_0^H \left(\frac{\partial M}{\partial T} \right)_H dH$$

For the magnetization data taken at discrete magnetic fields and temperatures, the above equation can be integrated numerically as [37],

$$\Delta S = \sum_i \frac{M_{i+1} - M_i}{T_{i+1} - T_i} \Delta H_i$$

where M_{i+1} and M_i are the measured magnetizations at temperatures T_{i+1} and T_i , respectively. The magnetization and ΔS_M , with respect to

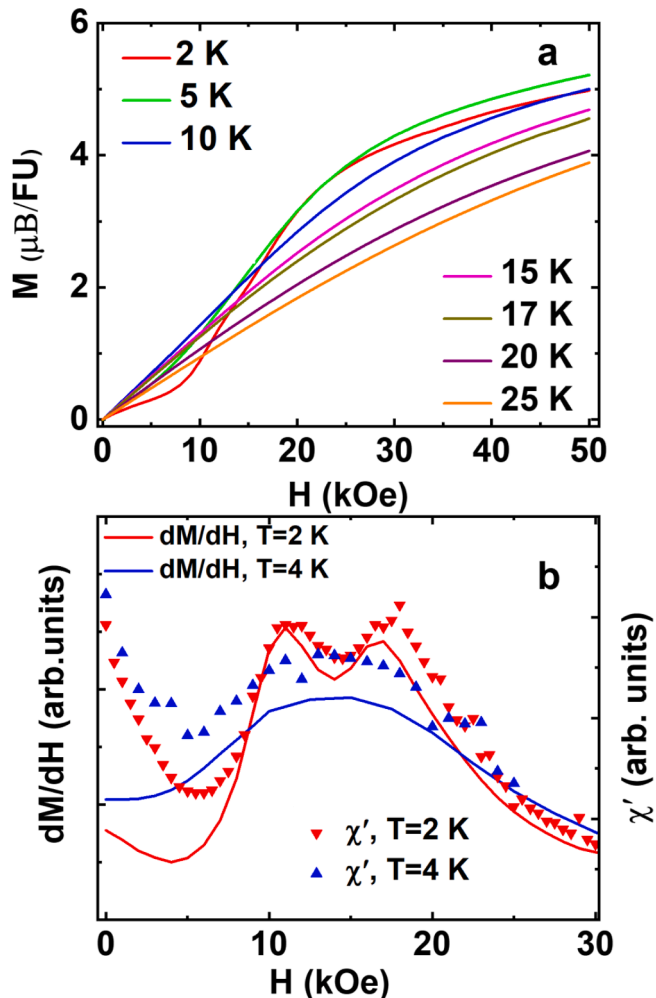


Fig. 3. (a) Magnetization, M , as function of magnetic field, H , for HoFeWO_6 . (b) Variation of dM/dH and χ' with H at $T = 2$ K and $T = 4$ K.

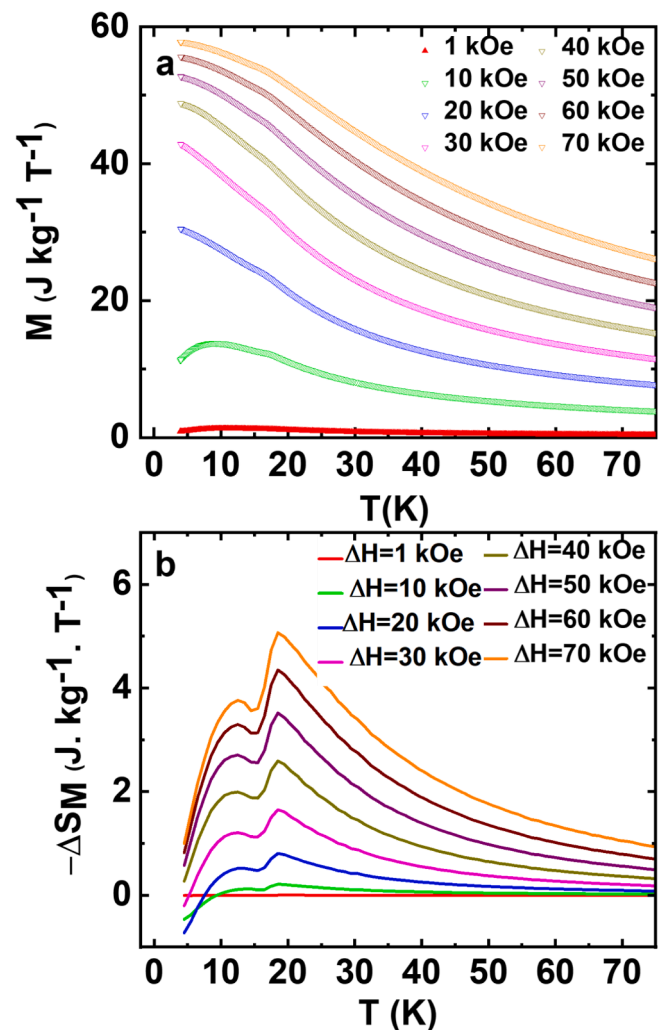


Fig. 4. (a) Magnetization vs temperature at indicated fields. (b) Magnetization data replotted as $-\Delta S_M$ versus T , using the relationships described in the main text.

temperature and field, are presented in Fig. 4 and supplementary section Fig. S2. It is clear from Fig. 4b that HoFeWO₆ shows double peaks in $-\Delta S_M$: a relatively sharp peak around 18 K and a field-dependent broad peak at lower temperatures. A magnetic entropy change of $\approx 5 \text{ J kg}^{-1} \text{ K}^{-1}$ occurs around the magnetic transition temperature at a field of 70 kOe. Such a presence of double peaks increases the working temperature range for magnetic refrigeration and the refrigerant capacity (RC). Quantitatively, the RC value is calculated as $RC = (\Delta S_M)(\Delta T_{\text{cycl}})$ [37,38] where ΔS_M is the value of entropy change at full width half maximum (FWHM) and $\Delta T_{\text{cycl}} = T_{\text{hot}} - T_{\text{cold}}$ is the temperature difference between two end points at FWHM. Taking $\Delta S_M = 2.5 \text{ J kg}^{-1} \text{ K}^{-1}$, and $T_{\text{cycl}} = T_{\text{hot}} - T_{\text{cold}} = 40 \text{ K} - 10 \text{ K} = 30 \text{ K}$, RC is 75 J kg^{-1} for a field change of 40 kOe. Such a value of RC is comparable to other members of this family [28–31] and manganites [37]. Therefore, this compound holds the potential to be used as a magnetocaloric material for cryogenic applications.

3.4. Magnetic structure determination

We also performed a temperature dependent neutron powder diffraction study of HoFeWO₆ to solve the magnetic structure of this compound. The diffraction data was collected at select temperatures above and below the magnetic transition temperature T_N . The neutron diffraction patterns between 25 K and 6 K were collected using bank 3 (central wavelength 2.665 Å) and the diffraction pattern at 2 K was collected using bank 2 (central wavelength 1.5 Å) on the POWGEN powder diffractometer. Due to the magnetic form factor, magnetic peaks are strongest in the low momentum transfer (low-Q or high-TOF) and disappear above the magnetic transition. Fig. 5a shows the development of one of the strongest magnetic peaks ($Q \approx 0.94 \text{ \AA}^{-1}$) with temperature. The variation of the integrated intensity of the peak with temperature (order parameter) is presented in Fig. 5b. The presence of this peak in the low-Q region and disappearance above T_N indicates this peak is purely magnetic in origin. We observed several magnetic peaks due to the large form factor associated with Ho³⁺ and Fe³⁺. Indexing of the extra peaks using FullProf program [32] gives the commensurate magnetic propagation vector $\mathbf{k} = (0, 0.5, 0.5)$, meaning the magnetic unit cell is double that of the crystallographic unit cell in both the *b* and *c* directions. The magnetic structure was determined using MAXMAGN [38] and Rietveld refinement using FullProf. There are 3 subgroups ($C_{4c} \# 9.41$, $P_{4c} \# 7.27$, and $Ps1 \# 1.3$) consistent with the $Pna2_1$ space group and the magnetic propagation vector. Out of these 3 magnetic space groups, the space group $C_{4c} \# 9.41$ best fits our data. We followed the procedure described in MAXMAGN [39] and reference [23] to transform from the parent like setting $[a, 2b, 2c; 0, 0, 0]$ to the standard Belov-Neronova-Smirnova (BNS) notation using the transformation $[c, b, -a; 0, 1/8, 0]$. Due to the monoclinic symmetry of the magnetic space group each of the Fe and Ho atoms split into two sites: Fe1, Fe2, Ho1,

and Ho2. The structural distortion caused by such splitting is negligibly small and beyond the resolution of our measurement. After the identification of the correct magnetic space group, the neutron diffraction data were refined by adding the nuclear and magnetic phases simultaneously. Fig. 6 presents the Rietveld refinement and the resulting magnetic structure at $T = 2 \text{ K}$. Table 1 summarizes the moment values of Fe1, Fe2, Ho1 and Ho2 at different temperatures. The net moment of Fe1 and Fe2 were constrained to be same. Similarly, the net moment of Ho1 and Ho2 were constrained to be same. The moments were refined in a spherical coordinate system where the magnitude of moments and angles (theta and phi) were refined freely. The variation of the magnitude of Fe and Ho moments with temperature are presented in Fig. 7, and the variation of the *x*, *y*, and *z* components (in Cartesian coordinates parallel to the lattice *a*-, *b*-, and *c*-axes, respectively) of Fe and Ho moments are presented Fig. 8. The Rietveld refinement at $T = 14 \text{ K}$ and the magnetic structures of the Fe and Ho sublattices at $T = 2 \text{ K}$ and $T = 14 \text{ K}$ are also presented in supplementary section (Figs. S3, S4, S5) [34].

There are many interesting features observed in the magnetic structure and its temperature variation. Although there are magnetic peaks at 16 K, due to its relatively low intensity we could not unambiguously solve the magnetic structure at this temperature. At 14 K (supplementary Fig. S3), the refinement gives a unique and stable solution only considering moments on both Fe and Ho sites. This indicates there is a development of an induced moment on Ho due to the ordering of Fe. The magnetic structure at 14 K indicates that the Fe spins are arranged in a strongly non-collinear and non-coplanar arrangement with 3-dimensional character, whereas the Ho moments are primarily confined to the *bc*-plane. On cooling down to 12 K, the Fe1 spins are primarily confined to the *ac*-plane whereas the Fe2 spins are confined to *bc*-plane, still forming a strongly non collinear spin structure. The variation of the ordered moment of Fe and Ho (Fig. 7) indicates that the ordered moment on Fe saturates to a value of $\approx 4 \mu_B$ around 12 K whereas the Ho moment increases monotonically acquiring the nearly free ion value of $\approx 8.7 \mu_B$ at 2 K. The ordered moment on Ho increases by almost $2 \mu_B$ from 6 K to 2 K. This may be due to the true ordering of Ho rather than an induced ordering by Fe.

A close look at the variation of the *x*, *y*, and *z* components of the moments (Fig. 8 and Table I), indicates that the Ho moments lie primarily within *bc*-plane at all temperatures, possibly due to a large single ion anisotropy associated with the Ho³⁺ ion, but the Fe moments have significant 3-dimensional character except at 2 K. At 2 K the Fe moments are also confined to *bc*-plane like the Ho moments. The Ho moments are large compared to the Fe moments, therefore, at low temperature, the Fe moments are also pulled toward the plane of Ho moments due to strong *3d-4f* coupling. The ordered moment of Fe at 2 K is $3.95 \pm 0.07 \mu_B$ whereas the ordered moment on Ho is $8.75 \pm 0.07 \mu_B$. These values are slightly less than the free ion values but are comparable to that of DyFeWO₆ [23]. Additionally, the strongly non-collinear and non-

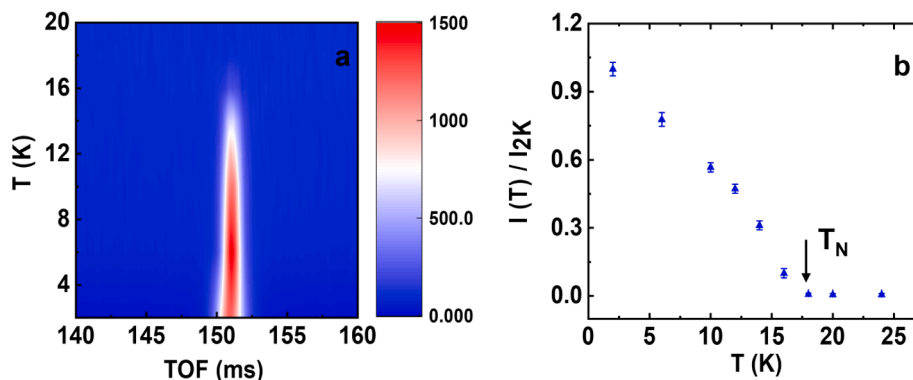


Fig. 5. (a) The evolution of one of the strongest magnetic peaks $[(1,1,1) + \mathbf{k}]$ with temperature. (b) The ratio of the integrated intensity at T with the integrated intensity at 2 K for the $(1,1,1) + \mathbf{k}$ magnetic Bragg peak.

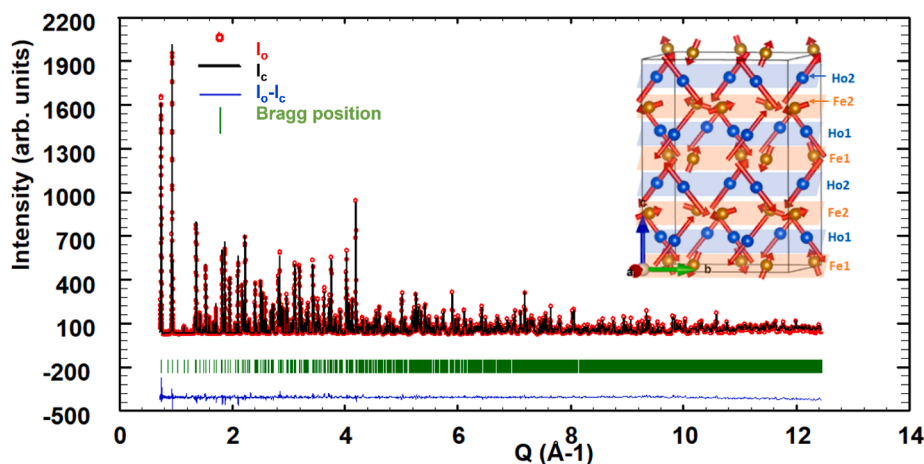


Fig. 6. Neutron diffraction data with Rietveld refinement on HoFeWO_6 at 2 K. The red dots represent observed data (I_o) and the black line represents the Rietveld fit to the data (I_c). The green ticks are the allowed nuclear and magnetic reflections (*Nuclear R-factor: 4.94, Magnetic R-factor: 1.89*). The inset shows the magnetic structure of HoFeWO_6 at 2 K.

Table 1

Components of magnetic moments (in μ_B) at different temperatures.

T (K)	Fe1			Fe2			Ho1			Ho2		
	Rx	Ry	Rz	Rx	Ry	Rz	Rx	Ry	Rz	Rx	Ry	Rz
2	0.51(16)	1.46(16)	3.63(10)	0.23(41)	3.76(9)	1.19(14)	0.78(31)	5.3(1)	6.85(7)	0.7(3)	5.33(7)	6.89(5)
6	1.78(16)	0.75(16)	3.64(10)	0.42(33)	3.69(11)	1.77(13)	0.21(23)	3.7(1)	5.46(6)	0.3(2)	4.22(6)	5.08(5)
10	1.82(18)	0.50(20)	3.39(11)	0.34(39)	3.37(12)	1.87(15)	0.12(24)	3.1(1)	4.54(7)	0.4(2)	3.53(8)	4.21(6)
12	1.69(19)	0.35(22)	3.06(13)	0.45(44)	2.98(15)	1.80(18)	0.20(25)	2.7(1)	3.79(8)	0.4(2)	2.93(9)	3.59(7)
14	1.53(24)	0.72(29)	2.39(16)	0.98(43)	2.47(25)	1.25(20)	0.02(26)	2.1(1)	2.9(1)	0.1(3)	2.13(11)	2.86(9)

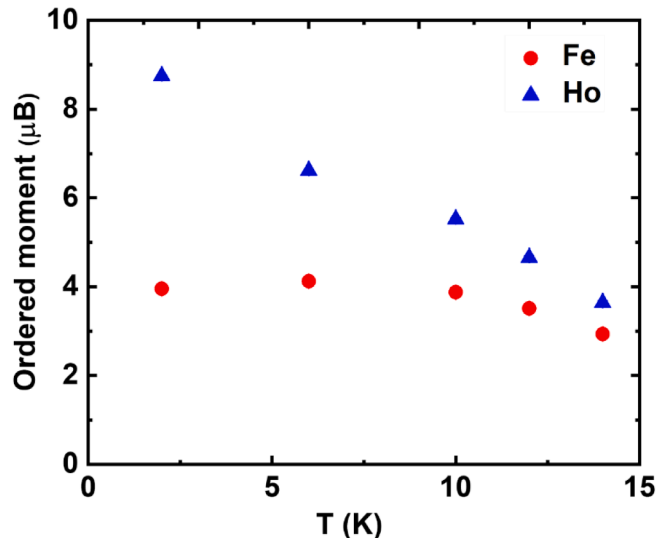


Fig. 7. Variation of ordered moments of Ho and Fe with temperature.

coplanar magnetic structure of HoFeWO_6 is similar to that of DyFeWO_6 [23] but differs from the collinear structures of HoCrWO_6 [28] and DyCrWO_6 [30].

4. Conclusion

The cation ordering of Fe^{3+} and W^{6+} in connected FeO_6 and WO_6 octahedra breaks the space inversion symmetry of the lattice resulting in the polar crystal structure of HoFeWO_6 , similar to other $R(\text{Fe}, \text{Cr}, \text{V})\text{WO}_6$ compounds [23–31]. Additionally, HoFeWO_6 exhibits decent

magnetocaloric properties with a significant working temperature range indicating its potential use as a low temperature magnetocaloric material. The magnetization behavior just below the ordering temperature T_N is consistent with the picture of induced ordering on the Ho site caused by the ordering of Fe. The broad peak in magnetic susceptibility (centered at T^*) might be related to the two-dimensional nature of Ho ordering. Here, the Ho moments are not ordered on their own but are induced ordered, with likely low-dimensional correlations influenced by the Fe atoms. At T^{**} , HoFeWO_6 exhibits a second magnetic transition as indicated by the susceptibility and the specific heat measurements. This transition is likely due to the true long-range ordering (not induced from Fe) of the Ho moments, which now more strongly influence the direction of the Fe moments.

The variation of the individual components of Fe1, Fe2, Ho1, and Ho2 (Fig. 8) indicate that the Fe moments form a strongly non-collinear and non-coplanar structure at or below T_N . Although the Ho moments are primarily confined to bc -plane at all temperatures, the Fe moments rotate continuously in the intermediate temperature range and finally are confined to the bc -plane along with the Ho moments at 2 K.

Now let us discuss the consequences of such magnetic ordering. The polar crystal structure of this compound allows for $(0, 0, p_z)$ -type polarization even at room temperature. However, due to the small value of polarization and averaging effect in polycrystalline samples, no polarization was detected at room temperature. As the temperature is cooled down to T_N , the symmetry of the magnetic structure ($C_{4c} \# 9.41$) allows for an additional polarization component along the x -direction with polarization type $(p_x, 0, p_z)$. Recent studies show the development of magnetic field dependent spontaneous polarization in HoFeWO_6 [25] and other $R\text{FeWO}_6$ [23,26] compounds below T_N . The spontaneous polarization below T_N was observed even in YFeWO_6 [23] (without a magnetic rare earth ion) while no detectable polarization was observed in RCrWO_6 [30] or RVWO_6 [29] compounds. Furthermore, the variation of the lattice parameters with temperature (supplementary Fig. S6)

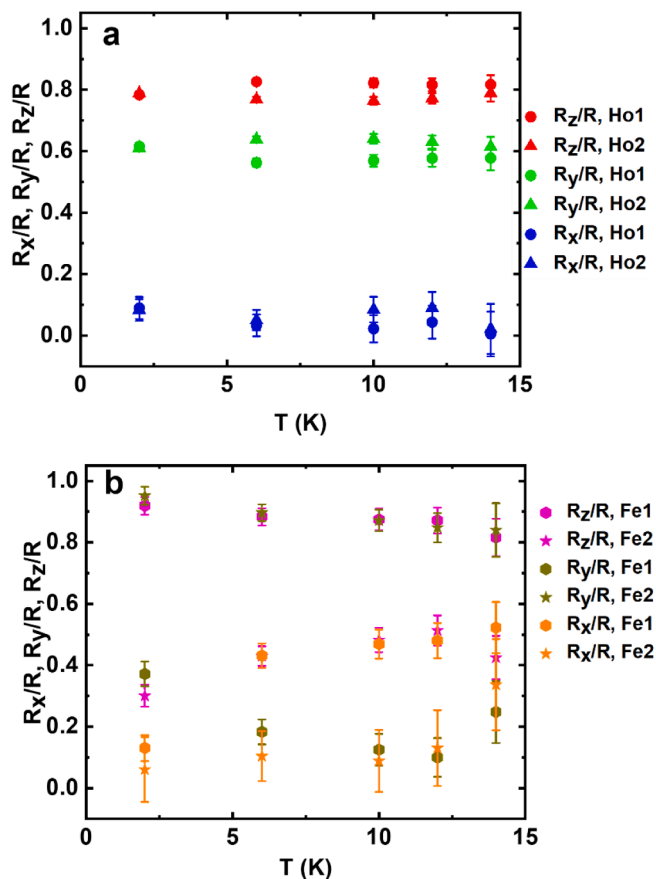


Fig. 8. Variation of the x , y , and z components of moments (a) for Ho and (b) for Fe with temperature. The components are divided by the total moment of that ion at that temperature.

exhibits no apparent discontinuity through T_N indicating the absence of any structural phase transition at T_N . The lattice parameters, however, change significantly between 6 K and 2 K. It might be an indication of magnetoelastic coupling or just the artifact of the different resolutions of bank 2 and bank 3 of the TOF diffractometer. Further synchrotron X-ray studies are desired for such understanding. All these facts indicate that the polarization in $RFeWO_6$ compounds is magnetic structure induced caused by strongly non-collinear and non-coplanar magnetic structure specific to the Fe sublattice. In $HoFeWO_6$, a slight decrease in polarization was also observed below 8 K. This is consistent with the observed magnetic structure of this compound, because below 6 K, the Fe moments are continuously pulled toward the plane of the Ho moments (bc -plane) and at 2 K both Fe and Ho moments lie primarily within the bc -plane with only small components along the a -axis.

In summary, our study investigates the temperature dependent magnetic structure evolution of $HoFeWO_6$ and explains the origin of the observed spontaneous polarization below T_N in this compound as well as in the $RFeWO_6$ family of compounds. Our work will provide future guidance for the choice of transition metal to achieve magnetic structure induced ferroelectric polarization in these compounds. While it is beyond the scope of this work now, it will be interesting to study the magnetic field dependent magnetic structure of this compound to understand why the polarization is suppressed in the presence of a magnetic field.

Declaration of Competing Interest

The authors declare that they have no known competing financial interests or personal relationships that could have appeared to influence

the work reported in this paper.

Acknowledgements

The work at Kennesaw State University was supported by faculty startup grant. Work at SUNY Buffalo State was supported by the National Science Foundation (Grant No. DMR-1406766). RN and RJ are supported by the U.S. Department of Energy (DOE) under EPSCoR Grant No. DE-SC0016315. A portion of this research used resources at the Spallation Neutron Source, a DOE Office of Science User Facility operated by the Oak Ridge National Laboratory. A portion of this work was performed at the National High Magnetic Field Laboratory, which is supported by National Science Foundation Cooperative Agreement No. DMR-1644779 and the State of Florida. The identification of any commercial product or trade name does not imply endorsement or recommendation by the National Institute of Standards and Technology.

Appendix A. Supplementary data

Supplementary data (The supplementary material contains the crystal structure as viewed from the different axes, the comparison of magnetic entropy using magnetization and heat capacity data, the Rietveld refinement at $T = 14$ K, the magnetic structures of the Fe and Ho sublattices, and the variation of lattice parameter with temperature) to this article can be found online at <https://doi.org/10.1016/j.jmmm.2021.168725>.

References

- [1] C. Rao, A. Sundaresan, R. Saha, *J. Phys. Chem. Lett.* 3 (2012) 2237.
- [2] C.A. Vaz, J. Hoffman, C.H. Ahn, R. Ramesh, *Adv. Mater.* 22 (2010) 2900.
- [3] N.A. Spaldin, M. Fiebig, *Science* 309 (2005) 391.
- [4] M. Bibes, A. Barthélemy, *Nat. Mater.* 7 (2008) 425.
- [5] S. Cheong, M. Mostovoy, *Nat. Mater.* 6 (2007) 13.
- [6] M. Fiebig, T. Lottermoser, D. Meier, M. Trassin, *Nat. Rev. Mater.* 1 (2016) 16046.
- [7] C. Ederer, N.A. Spaldin, *Phys. Rev. B* 71 (2005) 6.
- [8] B.B. Van Aken, T.T. Palstra, A. Filippetti, N.A. Spaldin, *Nat. Mater.* 3 (2004) 3.
- [9] R. Ramesh, *Nature* 461 (2009) 1218.
- [10] N.A. Spaldin, R. Ramesh, *Nat. Mater.* 18 (2019) 203.
- [11] W. Eerenstein, N.D. Mathur, J.F. Scott, *Nature* 442 (2006) 759.
- [12] Khomskii, *Physics* 2 (2009) 20.
- [13] Y. Tokura, S. Seki, N. Nagaosa, *Rep. Prog. Phys.* 77 (2014), 076501.
- [14] Y. Tokura, *J. Magn. Magn. Mater.* 310 (2007) 1145.
- [15] Y. Wang, G.L. Pascut, B. Gao, T.A. Tyson, K. Haule, V. Kiryukhin, S. Cheong, *Sci. Rep.* 5 (2015) 1.
- [16] T. Kurumaji, S. Ishiwata, Y. Tokura, *Phys. Rev. X* 5 (2015) 3.
- [17] T. Kurumaji, S. Ishiwata, Y. Tokura, *Phys. Rev. B* 95 (2017) 4.
- [18] V. Caignaert, A. Maignan, K. Singh, C. Simon, V. Pralong, B. Raveau, J.F. Mitchell, H. Zheng, A. Huq, L.C. Chapon, *Phys. Rev. B* 88 (2013) 17.
- [19] K. Singh, V. Caignaert, L.C. Chapon, V. Pralong, B. Raveau, A. Maignan, *Phys. Rev. B* 86 (2012) 2.
- [20] Y.S. Oh, S. Artyukhin, J.J. Yang, V. Zapf, J.W. Kim, D. Vanderbilt, S. Cheong, *Nat. Commun.* 5 (2014) 1.
- [21] I. Živković, K. Prša, O. Zaharko, H. Berger, *J. Phys.: Condens. Matter* 22 (2010) 5.
- [22] L. Zhao, C. Du, A.C. Komarek, *Phys. Status Solidi (RRL)–Rapid Res. Lett.* 11 (2017) 7.
- [23] S. Ghara, E. Suard, F. Fauth, T.T. Tran, P.S. Halasyamani, A. Iyo, J. Rodríguez-Carvajal, A. Sundaresan, *Phys. Rev. B* 95 (2017) 22.
- [24] R.S. Pn, S. Mishra, S. Athinarayanan, *APL Mater.* 8 (2020) 4.
- [25] M. Adnani, M. Gooch, L. Deng, S. Agrestini, J. Herrero-Martin, H. Wu, C. Chang, T. Salavati-Fard, N. Poudel, J.L. García-Muñoz, *Phys. Rev. B* 103 (2021) 9.
- [26] P. Yanda, S. Mishra, A. Sundaresan, *Phys. Rev. Mater.* 5 (2021) 7.
- [27] S.W. Kim, T.J. Emge, Z. Deng, R. Uppuluri, L. Collins, S.H. Lapidus, C.U. Segre, M. Croft, C. Jin, V. Gopalan, *Chem. Mater.* 30 (2018) 3.
- [28] C. Dhital, D. Pham, T. Lawal, C. Bucholz, A. Poyraz, Q. Zhang, R. Nepal, R. Jin, R. Rai, *J. Magn. Magn. Mater.* 514 (2020).
- [29] P. Yanda, A. Sundaresan, *Mater. Res. Express* 6 (2020) 12.
- [30] S. Ghara, F. Fauth, E. Suard, J. Rodríguez-Carvajal, A. Sundaresan, *Inorg. Chem.* 57 (2018) 20.
- [31] Y. Tian, J. Ouyang, H. Xiao, Y. Zhang, *Ceram. Int.* (2021).
- [32] J. Rodríguez-Carvajal, CEA/Saclay, France (2001).
- [33] G.J. Thorogood, M. Avdeev, B.J. Kennedy, *Solid State Sci.* 12 (2010) 1263.
- [34] Supplementary materials. This section contains crystal and magnetic structures as viewed along different crystallographic directions, magnetic entropy, and variation of lattice parameter with temperature.
- [35] K. Kittel, P. McEuen, *Introduction to Solid State Physics*, Wiley, New York, 1996, p. 8.

- [36] L. Ding, M. Lee, E.S. Choi, J. Zhang, Y. Wu, R. Sinclair, B.C. Chakoumakos, Y. Chai, H. Zhou, H. Cao, *Phys. Rev. Mater.* 4 (2020) 8.
- [37] M. Phan, S. Yu, *J. Magn. Magn. Mater.* 308 (2007) 325.
- [38] Q. Zhang, J.H. Cho, B. Li, W.J. Hu, Z.D. Zhang, *Appl. Phys. Lett.* 94 (2009), 182501.
- [39] J.M. Perez-Mato, S.V. Gallego, E.S. Tasci, L. Elcoro, G. de la Flor, M.I. Aroyo, *Annu. Rev. Mater. Res.* 45 (2015).